JOURNAL OF MATERIALS SCIENCE 28 (1993) 2915–2922

Effects of deposition temperature on the microstructure of MOCVD $Y_1Ba_2Cu_3O_{7-x}$ thin films

CHANGHYUN CHO, DOOSUP HWANG, KWANGSOO NO, J. S. CHUN
Department of Materials Science and Engineering, KAIST, Taejon 305-701 Korea
SANGHO KIM
Kia Technical Center, Kia Motor Co, Seoul, Korea

The effects of deposition temperature on the microstucture and composition of $Y_1Ba_2Cu_3O_{7-x}$ films deposited on MgO and $SrTiO_3$ substrates by the metal-organic chemical vapour deposition (MOCVD) method were investigated. As the deposition temperature decreased from 900 to 700 °C, the Cu content in the deposited film increased. SEM micrographs of the films showed that the growth direction of the film was changed from *c* axis to *a* axis perpendicular to the substrate surface, and then to random orientation, as the deposition temperature decreased. The superconducting transition temperature and the transition width of films deposited on $SrTiO_3$ substrates at temperatures higher than 810 °C were over 90 K and within 1 K, respectively.

1. Introduction

In 1987, Chu's group discovered high-T_c superconductivity above 90 K in the Y–Ba–Cu–O system [1]. After this discovery, many researches have been done on the mechanism and the application of this phenomenon. Observation of the superconducting phenomena was available with cheap liquid nitrogen, and the possibility of superconductivity in other oxide systems was shown. Bi–Sr–Ca–Cu–O and Ti–Ba–Ca–Cu–O systems were reported to show superconductivity above 110 K [2, 3].

The superconducting phase in the Y–Ba–Cu–O system is $Y_1Ba_2Cu_3O_{7-x}$ oxygen-deficient perovskite. The crystal structure consists of repeated $BaCuO_2$–$YCuO_{3-x}$–$BaCuO_2$ layers, and the superconductor shows anisotropic electrical properties [4]. When the superconductor is made using a conventional sintering technique, the grains in this material are randomly oriented. Even though the critical temperature is 90 K, the critical current density is about 10^3 A cm^{-2}. To achieve high critical current density, many studies on single-crystal growing and thin-film deposition were done. To make superconductor thin films, evaporation [5, 6], sputtering [7], metal-organic chemical vapour deposition (MOCVD) [8–10], and laser ablation [11] methods were investigated. Among these, the MOCVD method does not need a high vacuum and can be used in mass production.

Source materials for MOCVD are β-diketonate complexes ($Y(thd)_3$, $Ba(thd)_2$, $Cu(thd)_2$ where thd = 2,2,6,6,-tetramethyl 3,5-heptane). These materials sublimate above room temperature. The sublimation characteristics of the source powders affect the partial pressures of the source gases. So, studies on the sublimation characteristics of the source powders are needed to control the composition of the deposited film.

To achieve a high critical temperature and high critical density in superconducting Y–Ba–Cu–O films deposited using the MOCVD method, the following were studied: (i) the sublimation characteristics of the source powders $Y(thd)_3$, $Ba(thd)_2$ and $Cu(thd)_2$; (ii) the effects of deposition temperature on the concentration and microstructure of the film; and (iii) the relationship between microstructure and superconducting properties.

2. Experimental procedure

A schematic diagram of the deposition system is shown in Fig. 1. The apparatus can be divided into three subsystems: gas feed system, deposition system and pumping system. The gas feeding system consists of mass flow controllers (Unit Co.) and evaporators in which the source powders sublimate. The evaporator consists of three evaporation tubes (quartz, 15 mm inner dia.), one mixing tube (quartz, 25 mm inner dia.) and one oxygen feeding tube at the end of the mixing tube. All the tubes are heated using heating tapes, and the temperature of each evaporating tube is controlled using different temperature controllers. To minimize the possibility of condensation of the source material at the mixing tube, the temperature of the mixing tube was maintained at a temperature 10 °C higher than that of the evaporation tube. The deposition system consists of a reaction tube, a susceptor and a electric furnace. The reaction tube (quartz, 25 mm inner dia.) is connected to the mixing tube through a nozzle whose inner diameter is 13 mm. The susceptor is made of stainless steel, and a thermocouple is attached to one end of the susceptor in order to measure the substrate temperature. The pumping system consists of a rotary pump and a needle valve which controls reaction tube pressure.

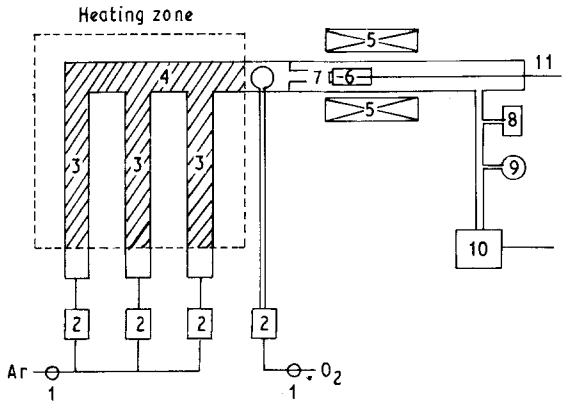

Figure 1 Schematic diagram of the MOCVD system: (1) air filter, (2) mass flow controller, (3, 4) evaporator, (5) furnace, (6) substrate holder, (7) substrate, (8) convection gauge, (9) compound gauge, (10) rotary pump, (11) thermocouple.

TABLE I Deposition conditions

Evaporation temperature	$Y(thd)_3$: 130–150 °C $Ba(thd)_2$: 230–280 °C $Cu(thd)_2$: 115–145 °C
Deposition temperature	750–900 °C
Deposition time	20 min, 1 h
Total Pressure	4 torr
Gas flow rate	Ar: 100 sccm O_2: 100 sccm
Substrate	MgO (1 0 0), $SrTiO_3$
Annealing process	Cooling rate: 4 °C min^{-1} (550 °C 30 min holding)

MgO (1 0 0) and $SrTiO_3$ (1 0 0) and (1 0 0) (10 mm × 10 mm × 1 mm) single-crystal plates were used for substrates. The source materials were $Y(thd)_3$, $Ba(thd)_2$ and $Cu(thd)_2$ powders. Each powder was weighed and evaporated in the evaporation tube, and the evaporated source was transported to the reaction tube with the Ar carrier gas. Table I shows the deposition conditions. Before the deposition process, the reaction tube was purged with Ar gas. Oxygen gas was added to decompose the organic chelate and to oxidize the deposited film.

The deposited film was annealed *in situ* at 1 atm oxygen. After the deposition, the film was cooled to 550 °C with 4 °C min^{-1} cooling rate, and held at 550 °C for 30 min. After annealing, the film was furnace-cooled to room temperature.

Energy-dispersive X-ray spectroscopy (EDS) was used to analyse the composition of the deposited film and the ZAF correction technique was used for quantitative analyses. The phase of the deposited film and the orientation was determined by X-ray diffraction. The texture coefficient was calculated using Harris method:

$$TC(hkl) = \frac{I(hkl)/I_0(hkl)}{(1/N)\sum[I(hkl)/I_0(hkl)]} \quad (1)$$

where $TC(hkl)$ = texture coefficient of plane (hkl), $I(hkl)$ = measured X-ray intensity of plane (hkl), $I_0(hkl)$ = standard X-ray intensity of plane (hkl) and N = number of reflections.

The microstructure of the deposited film was observed using scanning electron microscopy (SEM). The critical temperature was measured using a conventional four-probe method.

3. Results and discussion

3.1. Evaporation characteristics of the source powders

To study the evaporation characteristics of the source powders, the evaporation temperature and time were varied in the deposition process. Fig. 2 shows relationships between the evaporation rate of the source and

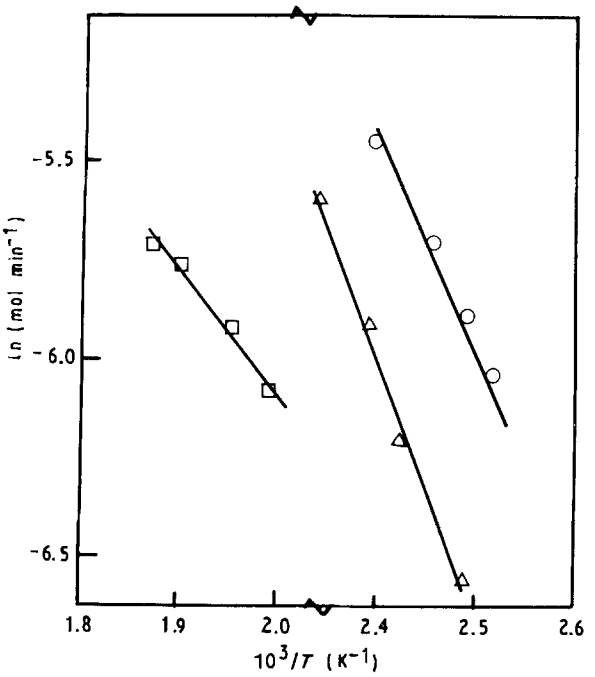

Figure 2 Relationship between evaporation rates of the source powders and temperature for the three source powders (carrier gas: Ar, 100 sccm for each). (△) $Y(thd)_3$, (□) $Ba(thd)_2$, (○) $Cu(thd)_2$.

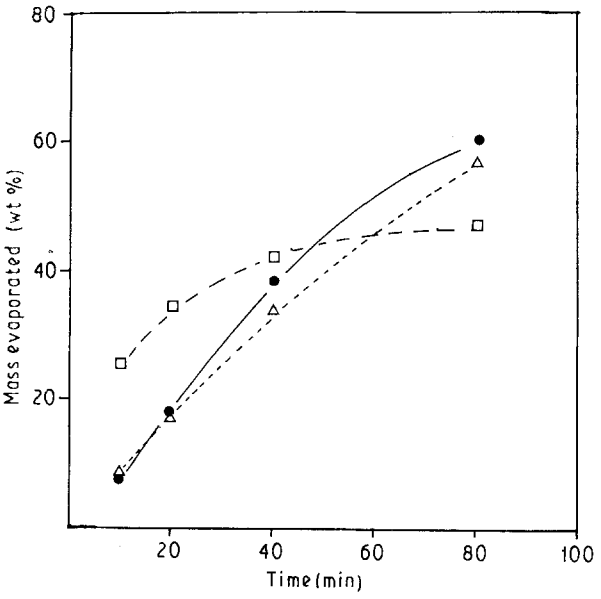

Figure 3 Relationship between evaporated weight percentage of the source powder and time (carrier gas: Ar, 100 sccm for each). (△) $Y(thd)_3$, (□) $Ba(thd)_2$, (●) $Cu(thd)_2$.

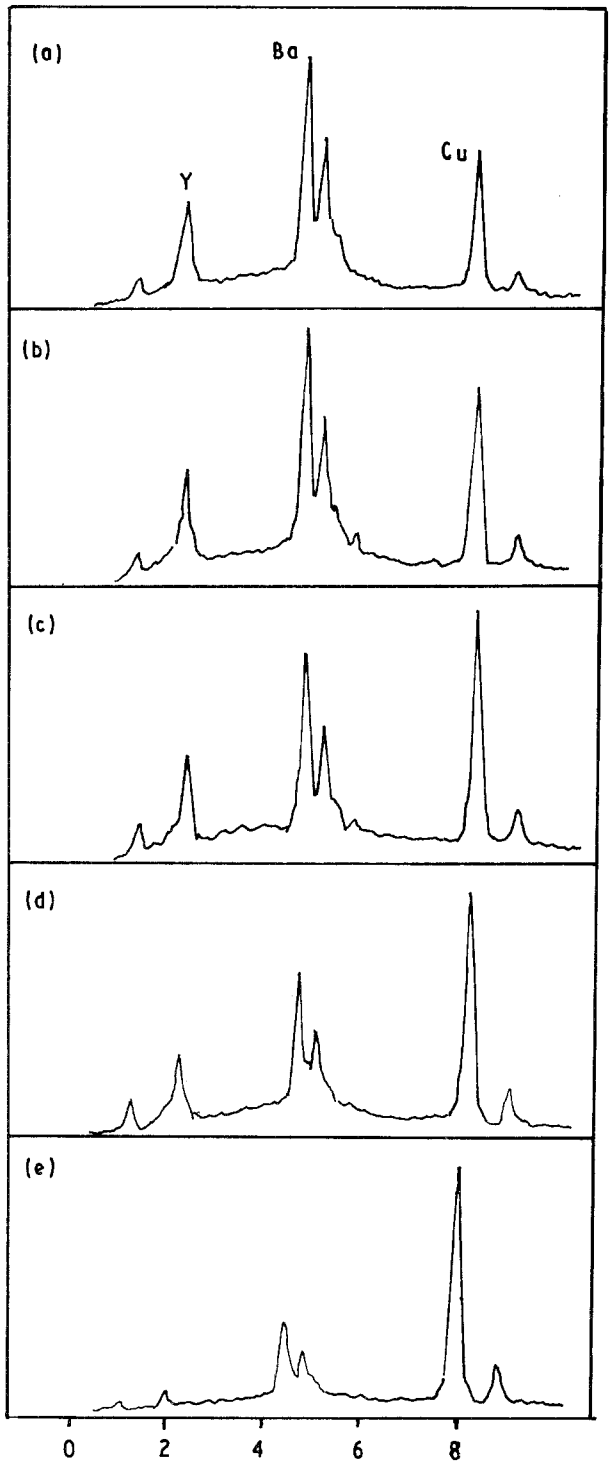

Figure 4 EDS spectra of YBaCuO films deposited at different temperatures (substrate MgO): (a) 900 °C, (b) 870 °C, (c) 840 °C, (d) 810 °C, (e) 780 °C.

temperature for the three source powders. When a solid is in equilibrium with vapour, the Gibbs free energy of species i can be represented as

$$G_i = RT\ln(P_i) \quad (2)$$

where G_i = Gibbs free energy of species i, P_i = partial pressure of species i and R = gas constant. At a certain temperature T, the vapour pressure of species i is

$$P_i = A\exp(-E_{ai}/RT) \quad (3)$$

where E_{ai} = sublimation activation energy of species i and A = a constant containing a geometrical factor.

Equation 3 shows that the temperature dependence of the vapour pressure will be large when the activation energy of the sublimation is large. From the slope of the lines in Fig. 2, the activation energies of the sublimation were 212.8, 153.2 and 198.6 kJ mol^{-1} for $Y(thd)_3$, $Ba(thd)_2$ and $Cu(thd)_2$, respectively. The Ba source showed relatively small dependency on the evaporation temperature.

To minimize the possibility of condensation and decomposition of the source vapour in the mixing tube, the temperature of the mixing tube was maintained 10 °C higher than that of the evaporation tube. If loss of the source vapour is negligible until they reach the reaction tube, the partial pressure of the source vapour is proportional to the evaporation rate of the source powder. The partial pressure of source vapour at time t_1 can be expressed as

$$P_i(t = t_1) = K\frac{1}{M_i}\left(\frac{dm_i}{dt}\right)t_1, \quad (4)$$

where K = a proportionality constant, p_i = partial pressure of source i, M_i = molar weight of source i and m_i = mass of source i.

Fig. 3 shows the relationship between the evaporated mass and evaporation time for the three source powders. For Y and Cu sources the evaporated mass showed a linear relationship with evaporation time, but for the Ba source the evaporated mass rate decreased after 40 min. This degradation of the Ba source was observed at different evaporation temperatures. The reason for the degradation may be due to the polymerization of the source material. Matsuno *et al.* [12] also observed the degradation of $Ba(thd)_2$, and they solved this problem by the addition of tetrahydrofuran to the Ar carrier gas. The partial pressure of the source vapour was controlled by changing the vaporization temperature of the source powder, which affects the concentration of the deposited film when the film is deposited in a diffusion-controlled region. To avoid the problem caused by

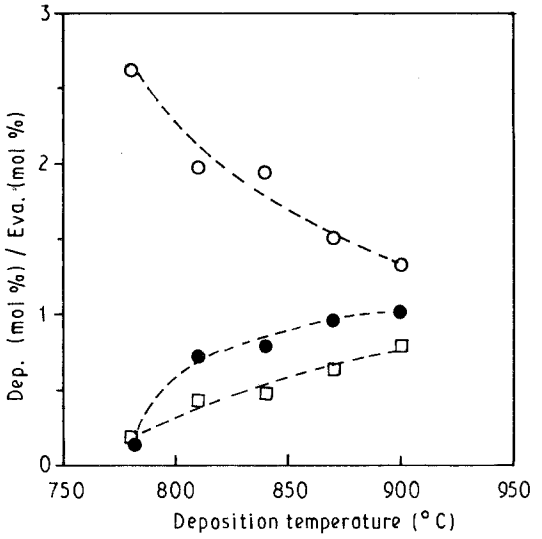

Figure 5 Ratios of the deposited mole percentage to the evaporated mole percentage of films deposited at different temperatures: (●) Y, (□) Ba, (○) Cu.

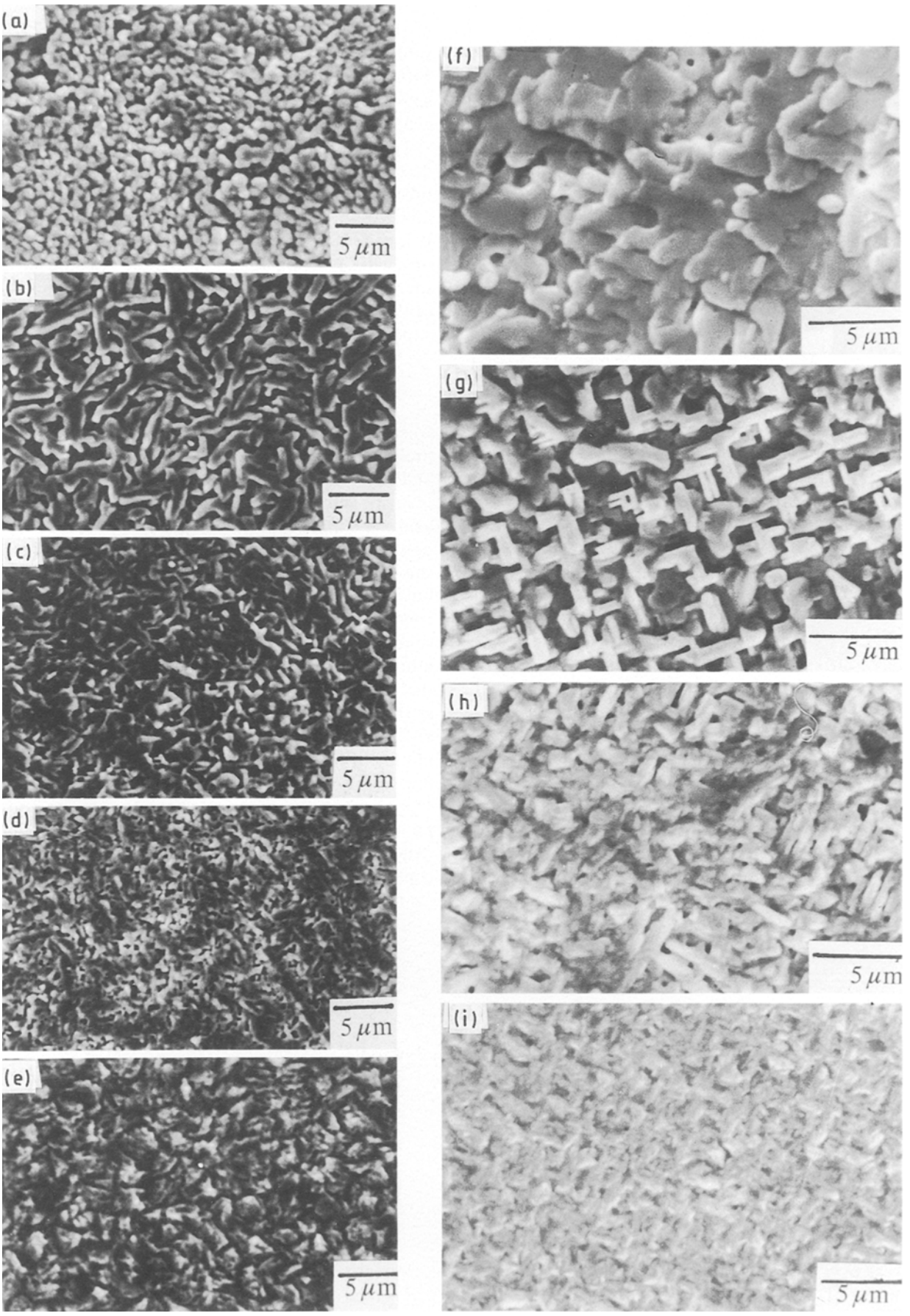

Figure 6 Surface morphology of YBaCuO films deposited on MgO and $SrTiO_3$ at different deposition temperatures. MgO: (a) 900 °C, (b) 870 °C, (c) 840 °C, (d) 810 °C, (e) 780 °C. $SrTiO_3$: (f) 870 °C, (g) 840 °C, (h) 810 °C, (i) 780 °C.

degradation of the Ba source, the deposition time was limited to 20 min for MgO substrates and 30 min for $SrTiO_3$ substrates.

3.2. Composition of the deposited film

Fig. 4 shows EDS spectra of the deposited films at different deposition temperatures. As the deposition temperature decreased the Cu concentration increased. Fig. 5 shows the ratio of the deposited mole percentage to the evaporated mole percentage of the three sources at different temperatures. As shown in Fig. 4, the deposition ratio of Cu increased as the deposition temperature decreased. The reason for the increase of Cu in the deposited film at lower temperature is due to either an increase of the adsorption coefficient of Cu atoms or a decrease of the predecomposition of Cu source vapour in the prereaction region.

3.3. Microstructure and X-ray diffraction

Fig. 6 shows SEM micrographs of the films deposited on different substrates and at different temperatures.

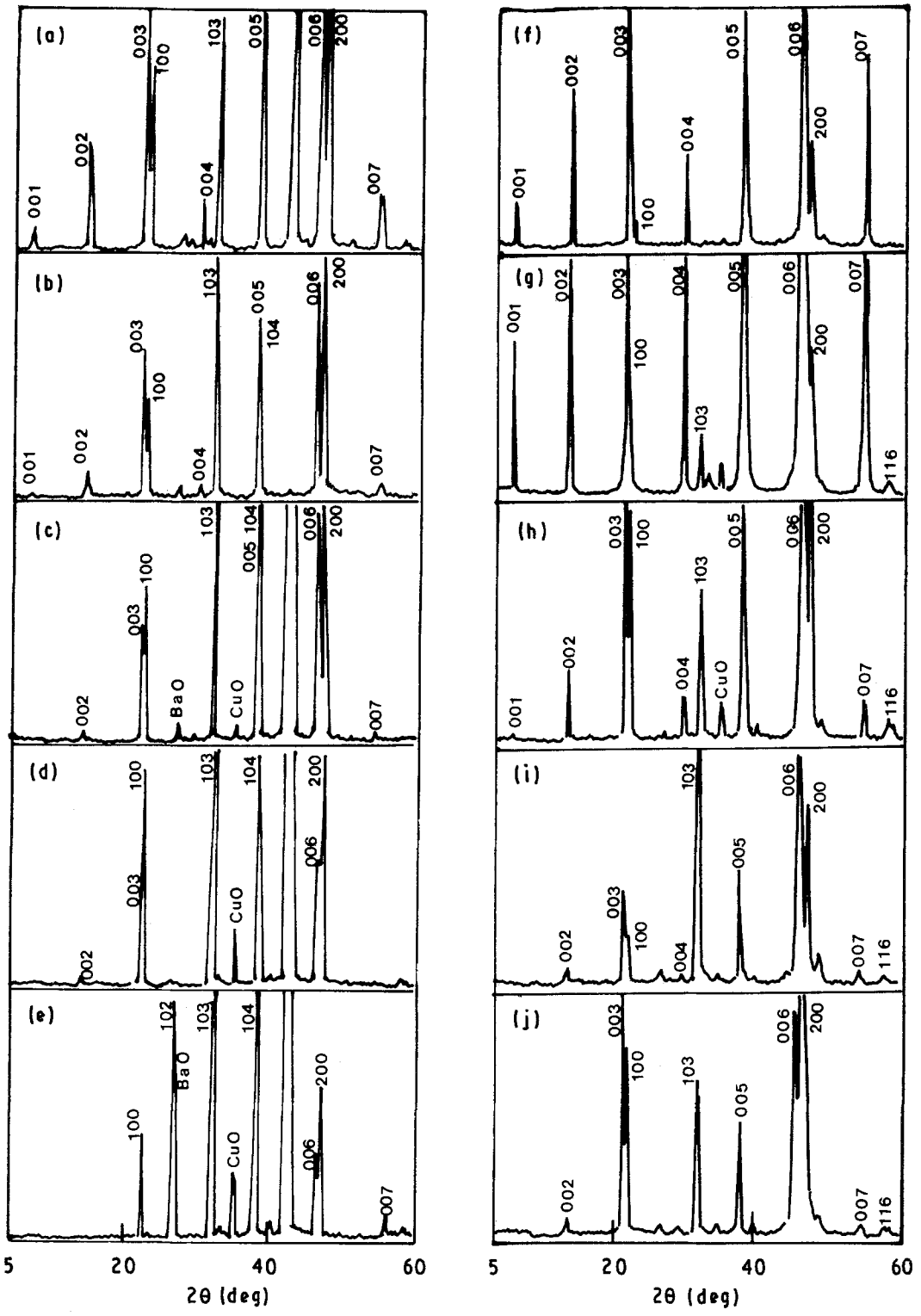

Figure 7 X-ray diffraction patterns of YBaCuO films deposited on MgO and $SrTiO_3$ at different deposition temperatures. MgO: (a) 900 °C, (b) 870 °C, (c) 840 °C, (d) 810 °C, (e) 780 °C. $SrTiO_3$: (f) 870 °C, (g) 840 °C, (h) 810 °C, (i) 780 °C, (j) 750 °C.

The grain size of the film increased as the deposition temperature increased. The film shows dense microstructure at relatively low deposition temperature. When the film was deposited on an MgO substrate at 900 °C, the grain shape was near-spherical. When the deposition temperature was lowered to 800 °C, long grains were observed on the MgO substrate. On $SrTiO_3$ substrates, plate-shaped grains were observed at relatively higher deposition temperature, which indicates that the *c* axis of the grain was normal to the substrate. As the deposition temperature decreased, long grains appeared on the microstructure, which indicates that the *c* axis of the grain became parallel to the substrate surface.

The shape of the grain was controlled by the mobility of the atoms at the substrate surface and the surface energy anisotropy of the grain. At high deposition temperature, the mobility increased and the *a–b* plane grew parallel to the substrate surface. It has been reported that the growth rate of the *a* and *b* directions is larger than that of the c direction. As the deposition temperature decreased, the surface mobility of the adsorbed atoms decreased. So, the grain growth rate was reduced, and the growth direction of the *a*, *b* axis became normal to the substrate surface. If the deposition temperature was lower than 800 °C the grain shape was hard to observe, and the surface of the deposited film was smooth.

Fig. 7 shows X-ray diffraction patterns of the films deposited on different substrates and at different temperatures. On MgO substrates, no major impurity-phase peak was detected at the deposition temperature of 900 °C. As the deposition temperature decreased, a $BaCuO_2$ impurity peak appeared. When the deposition temperature was lower than 800 °C, BaO and CuO peak appeared. On $SrTiO_3$ substrates, (0 0 1) peaks were dominant on the films deposited at relatively high temperatures. As the deposition temperature decreased, (*h* 0 0) peaks appeared. Only CuO was detected as an impurity phase at low deposition temperature.

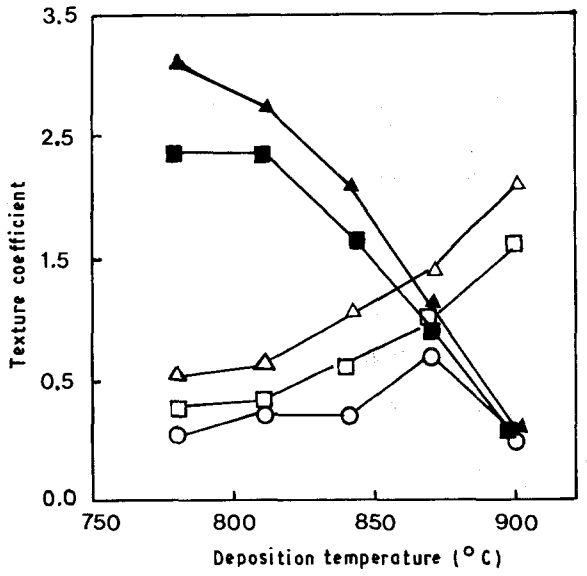

Figure 8 Variation of texture coefficient of YBaCuO films deposited at different temperatures (substrate MgO): (□) (0 0 2), (△) (0 0 5), (■) (1 0 0), (▲) (2 0 0), (○) (1 0 3).

TABLE II Texture coefficients of the film at different deposition temperatures (substrate MgO (1 0 0) single crystal)

	Deposition temperature (°C)				
hkl	900	870	840	810	780
0 0 2	1.60	0.98	0.62	0.28	0.27
0 0 3	2.11	1.40	1.03	0.62	0.52
1 0 0	0.02	0.90	1.71	2.37	2.37
1 0 3	0.02	0.72	0.21	0.26	0.03
0 0 6	1.59	0.92	0.67	0.50	0.49
2 0 0	0.07	1.08	2.12	2.76	3.09
0 0 7	1.59	0.99	0.64	0.21	0.23

Table II and Fig. 8 show texture coefficients of the deposited films calculated from the data of Fig. 7. The standard value of X-ray peak was taken from the data of Wong-Ng and Roth [13]. The lattice parameter of the $SrTiO_3$ crystal is 0.39 nm, which is the same as one-third of the *c* axis lattice in the $Y_1Ba_2Cu_3O_{7-x}$ crystal. Those peaks were excluded when we calculated the texture coefficient. As the deposition temperature decreased, (*h* 0 0) peaks appeared dominantly. At low deposition temperatures, the surface mobility of adatoms decreased and grains whose *a*, *b* axis was normal to the substrate were observed.

3.4. Critical temperature and critical current density

Fig. 9 shows temperature versus resistivity plots of the films deposited on different substrates and at different temperatures. The films on MgO substrates showed a lower critical temperature at higher deposition temperature. The transition width (difference between $T_{c(onset)}$ and $T_{c(zero)}$ decreased as the deposition temperature decreased. The films deposited at 900 °C showed metallic resistivity behaviour, but $T_{c(zero)}$ was lower than 60 K. The films on $SrTiO_3$ substrates showed a $T_{c(zero)}$ of 90 K, and the critical temperature transition width was lower than 1 K. When the deposition temperature decreased to 800 °C the transition width increased; $T_{c(onset)}$ was 90 K and $T_{c(zero)}$ was 82 K.

The films on MgO substrates showed a low critical current density of 10^3 A cm^{-2} at 77 K. Fig. 10 shows critical current density versus deposition temperature plots of the films on $SrTiO_3$ substrates. The critical current density of the film deposited on $SrTiO_3$ at 840 °C was about 10^6 A cm^{-2} at 77 K. The observed high critical current density may be due to epitaxial growth of the film as shown in the microstructure.

4. Conclusions

Y–Ba–Cu–O superconducting thin films were deposited on MgO (1 0 0) and, $SrTiO_3$ (1 0 0) substrates using the MOCVD method. The effects of deposition temperature on the microstructure and on the superconducting properties were observed. From the results, we obtained the following conclusions:

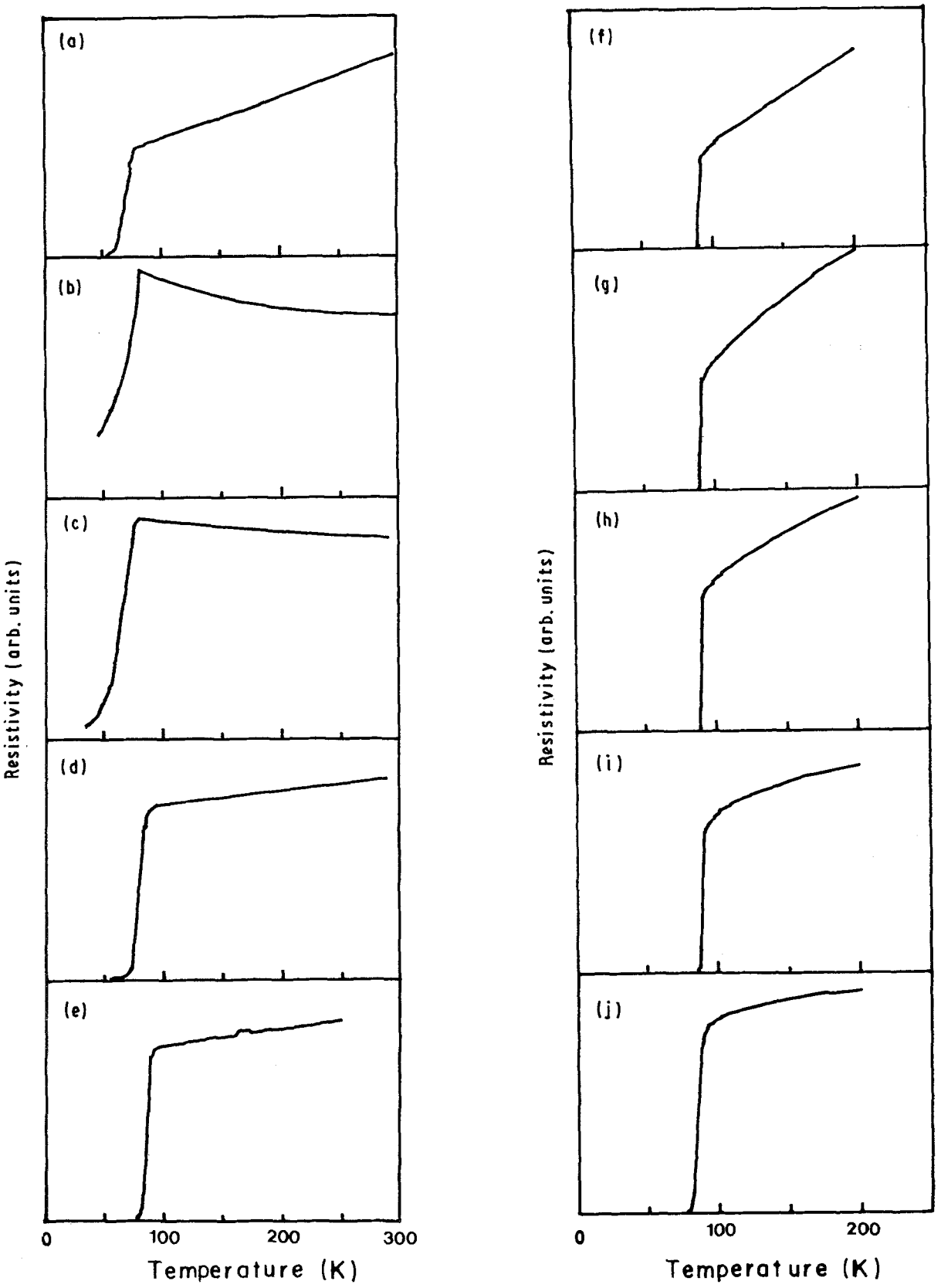

Figure 9 Temperature versus resistivity plots of YBaCuO films deposited on MgO and $SrTiO_3$ at different deposition temperatures. MgO: (a) 900 °C, (b) 870 °C, (c) 840 °C, (d) 810 °C, (e) 780 °C. $SrTiO_3$: (f) 870 °C, (g) 840 °C, (h) 810 °C, (i) 780 °C, (j) 750 °C.

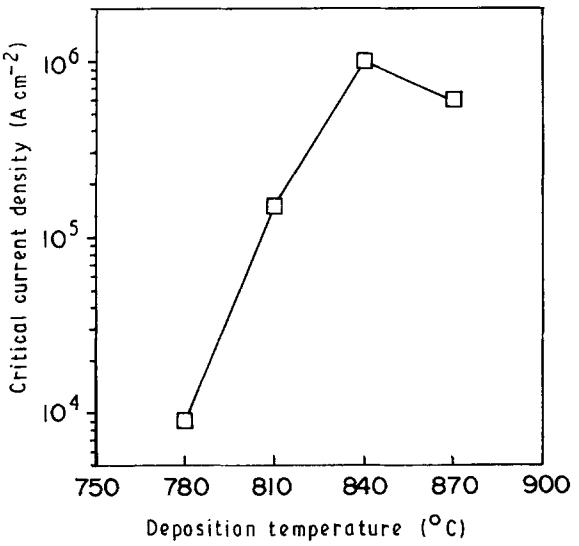

Figure 10 Critical current density of YBaCuO films deposited on $SrTiO_3$ (1 0 0) single crystal.

1. The preferred orientation of $Y_1Ba_2Cu_3O_{7-x}$ film changed from (0 0 *l*) to (*h* 0 0) as the deposition temperature decreased.

2. The Cu content in $Y_1Ba_2Cu_3O_{7-x}$ films increased at relatively low deposition temperature, and impurity phases were observed in the films deposited on MgO substrates.

3. The critical temperature of $Y_1Ba_2Cu_3O_{7-x}$ films was dependent on the substrate. On MgO substrates the critical temperature increased as the deposition temperature decreased. On $SrTiO_3$ substrates most films showed a $T_{c(zero)}$ of 90 K, and the transition width was less than 1 K.

References

1. M. K. WU, J. R. ASHBURN, C. J. TRONG, P. H. HOR, R. L. MENG, L. GAO, Z. J. HUANG. Y. Q. WANG and C. W. CHU. *Phys. Rev. Lett.* **58** (1987) 908.
2. H. MAEDA, Y. TANAKA, M. HUKUTOMI and T. ASANO, *Jpn J. Appl. Phys.* **27** (1988) L209.
3. Z. Z. SHENG and A. M. HERMANN, *Nature* **332** (1988) 55.
4. P. K. GALLAGHER, H. M. O'BRYAN, S. A. SUNSHINE and D. W. MURPHY, *Mater. Res. Bull.* **22** (1987) 995.
5. S. MIURA. T. YOSHITAKE, T. SATOH, Y. MIYASKA and N. SHOHAT, *Appl. Phys. Lett.* **52** (1988) 1008.
6. K. TERASHIMA, K. EGUCHI. T. YOSHICA and K. AKASHI, *ibid.* **52** (1988) 1274.
7. J. W. C. de VRIES, B. PAM, M. G. J. HEIJAM. G. M. STOLLMAN and M. A. M. GIJS, *ibid.* **52** (1988) 1904.
8. F. SCHMADERER and G. WAHL, *J. Physique* **50** (1989) 119.
9. H. ABE. T. TSURUOKA and T. NAKAMORI, *Jpn J. Appl. Phys.* **27** (1988) L1473.
10. A. J. PANSON, R. G. CHARLES. D. N. SCHMIDT, J. R. SZEDON, G. J. MACHIKO and A. I. BRAGINSKI, *Appl. Phys. Lett.* **53** (1988) 1756.
11. M. R. RAO, E. J. TARSA, L. A. SAMOSKA, J. M. ENGLISH, A. C. GOSSARD, H. KROEMER, P. M. PETROFF and E. L. HU, *ibid.* **56** (1990) 1905.
12. S. MATSUNO, F. UCHIKAWA and K. YOSHIZAKI, *Jpn J. Appl. Phys.* **29** (1990) L947.
13. WONG-NG and W. ROTH, *Adv. Ceram. Mater.* **2(3B)** (1987) 565.

Received 16 December 1991
and accepted 2 September 1992